A New Conjugate Gradient Method and Application to Dynamic Load Identification Problems

Lin J. Wang

Hubei Key Laboratory of Hydroelectric Machinery Design and Maintenance, College of Mechanical and Power Engineering, China Three Gorges University,Yichang, Hubei 443002, PR China.
School of Chemistry, Physics and Mechanical Engineering, Queensland University of Technology, Brisbane, QLD 4001, Australia. E-mail: ljwang2006@126.com.

Xiang Gao

Hubei Key Laboratory of Hydroelectric Machinery Design and Maintenance, College of Mechanical and Power Engineering, China Three Gorges University,Yichang, Hubei 443002, PR China.

You X. Xie

College of Science Technology, China Three Gorges University, Yichang, P.R. China.

Jun J. Fu and Yi X. Du

Hubei Key Laboratory of Hydroelectric Machinery Design and Maintenance, College of Mechanical and Power Engineering, China Three Gorges University,Yichang, Hubei 443002, PR China.

(Received 30 October 2020; accepted 20 February 2021)

In this paper, a modified conjugate gradient (MCG) algorithm is proposed for solving the force reconstruction problems in practical engineering. This new method is derived from a stable regularization operator and is also strictly proved using the mathematical theory. Moreover, we also prove the sufficient descent and global convergence characteristic of the newly developed algorithm. Finally, the proposed algorithm is applied to force reconstruction for the airfoil structure and composite laminated cylindrical shell. Numerical simulations show that the proposed method is highly efficient and has robust convergence performances. Additionally, the accuracy of the proposed algorithm in identifying the expected loads is satisfactory and acceptable in practical engineering.

1. INTRODUCTION

In recent years, force identification in structural dynamics has attracted lots of interest of many scholars.[1–7] The inverse force identification by structural vibration data such as displacement responses is particularly suitable for structural mechanics and structural health monitoring in the field of mechanical engineering. However, for a great many practical engineering problems, we have to try our best to know the corresponding information of external loads. For example, after knowing external force acting on the structure of aircraft wings and wind turbines, it is possible or convenient to exploit a great many advanced computational algorithms to ensure their safety. Also, we often optimize these structures to satisfy the requirements of industrial development. Moreover, in many cases, it is not easy to get the accurately applied loads thatact on engineering structures, so efforts are made to develop indirect computational inverse technology which computes the excitation loads with known vibration data, such as displacement responses, strain data, and acceleration and velocity responses.[8–10]

Jacquelin et al. analyzed a deconvolution technique and successfully used this method to recover an experimental force.[11] The finite element method is exploited to reconstruct the moving loads acting on the bridge deck.[12] Gunawan et al. proposed the Two-step B-splines regularization method and used it to regularize the ill-posed problem of impact load reconstruction.[13] Zhu and Law exploited a new algorithm that is based on the regularization method and modal superposition and applied it for the moving force reconstruction.[14] A regularization method using signal processing techniques was proposed to deal with force identification.[15] The dynamic programming algorithm was exploited by Law et al. to identify the moving force.[16] Zhang and Ohsaki transformed the force reconstruction for the prestressed pin-jointed structure into an optimization problem and solved it using the method of simulated annealing method.[17] Xie et al. proposed an identification method based on statistical energy analysis to solve the high-frequency load identification.[18] Li et al. presented a new method that uses wavelet multi-resolution analysis to solve the load identification.[19] A novel load identification method was proposed to deal with the identification of discontinuous loading.[20]

However, there are still some shortcomings that exist in the research study so far. Firstly, the results of most traditional methods are weak anti-noise in identifying multi-source dynamic loads and are still not satisfactory when the noisy level increases. Additionally, we often use the iterative regularization method to obtain the solution of large-scale inverse problems, but their convergence rate in obtaining a regularized solution is pretty slow and inefficient.[21] Furthermore, very few references are found about the load identification in the aspect of large noisy levels.[22–24] Therefore, we have to seek new advanced computational methods to overcome these shortcomings. A new fast and efficient conjugate gradient method is presented in this paper, also proved by mathematical theory, and exploited to reconstruct dynamic load in the time domain from measured displacement responses.

This paper proceeds as follows. Section 2 devotes to the establishment of the new fast and efficient conjugate gradient algorithm. The sufficient descent characteristic and global attractivity of the proposed method are strictly proved in Section 3. In Section 4, we present numerical studies to investigate the stability, accuracy, and effectiveness of the newly developed method. The performances of the proposed method under different measurement noisy levels are investigated in detail. Finally, the last section presents the conclusions of this paper.

2. THE CONSTRUCTION OF A NEW FAST AND EFFICIENT CONJUGATE GRADIENT ALGORITHM

Firstly, the following unconstrained optimization problem is investigated:

$$\min_{x\in R^n} f(x); \tag{1}$$

in which $f : R^n \to R$ is a continuous and differentiable function. At point x_k, its gradient is denoted by $g(x_k)$. The corresponding iteration form is given as

$$x_{k+1} = d_k\alpha_k + x_k, k = 0, 1, 2\cdots; \tag{2}$$

in which α_k denotes the steplength and the search direction is denoted by d_k. Usually, the one-dimensional search method is used to search the stepsize, and the corresponding formula is defined as

$$f(d_k\alpha_k + x_k) = \min_{\alpha\geq 0} f(d_k\alpha_k + x_k); \tag{3}$$

where d_k represents the search direction given by the following equation:

$$d_k = \begin{cases} -g_0, & k{=}0, \\ d_{k-1}\beta_k - g_k, & k\geq 1 \end{cases}; \tag{4}$$

in which β_k is a scalar, and scientific and reasonable choices for this parameter correspond to different kinds of new conjugate gradient methods. Herein, a new formula for this parameter is given by

$$\beta_k^{WDX} = \begin{cases} \frac{g_k^T d_k}{g_k^\alpha d_{k-1}}(\alpha\geq 1) & if\ \|g_k\|\geq 1 \\ 1 & \text{otherwise} \end{cases}. \tag{5}$$

The corresponding new algorithm is given as the following steps:

MCG Algorithm

Step 0: Considering $x_0 \in R^n$, set $k = 0$.
Step 1: Obtain β_k using the formula Eq. (5).
Step 2: Compute d_k on the basis of Eq. (4). When $\|g_k\| <\varepsilon$, then stop.
Step 3: Generate α_k exploiting Eq. (3).
Step 4: Renewing next point according to Eq. (2). We will stop it when $\|g_k\| < \varepsilon$ and $f(x_k) > f(x_{k+1})$ or else go to Step 0 with $k = k + 1$.

3. GLOBAL CONVERGENCE

The validity and convergence of new parameter β_k^{WDX} will be investigated in the following part. To prove the good definition of the corresponding new algorithm for the new parameter, we will investigate its global convergence.

Theorem 3.1. Considering the conjugate gradient algorithm based on the new parameter β_k^{WDX}, Eqs. (3) and (4), then we have that there is $C > 0$ such that

$$g_k^T d_k \leq -C\|g_k\|^2; \tag{6}$$

when $k \geq 0$.

Proof. Firstly, we can easily obtain the assertion when $k = 0$. Secondly, the statement that the sufficient condition is also true for $k \geq 1$ will be strictly proved.

Using Eq. (4), we can get

$$g_{k+1}^T d_{k+1} = \\ g_{k+1}^T(-g_{k+1}+\beta_{k+1}d_k) = -\|g_{k+1}\|^2+\beta_{k+1}g_{k+1}^T d_k. \tag{7}$$

We also easily obtain that $g_{k+1}^T d_k = 0$ according to the exact line search. Then, we can obtain that

$$g_{k+1}^T d_{k+1} = -\|g_{k+1}\|^2.$$

Therefore, we can assert that d_{k+1} is a feasible direction. Thus, the proof of Theorem 3.1 is completed.

(H1). For the level set R^n, there is a lower bound for f; For x_0 given, there exists a neighborhood N of $\Gamma=\{x \in R^n | f(x_0) \geq f(x)\}$ in which f is continuously differentiable.

(H2). There is $L > 0$ such that

$$\|g(y) - g(x)\| \leq L\|y - x\|, \forall x, y \in N;$$

i.e., $g(x)$ is Lipschitz continuous.

Exploiting (H1) and (H2), we can get the following assertions [25, 26]:

Lemma 3.1 Suppose (H1)-(H2) are satisfied. Considering any conjugate gradient method by Eq. (4), in which α_k meets the precise minimization rule and d_k represents a descent search direction. Therefore,

$$\sum_{k=0}^{\infty}\frac{g_k^T d_k}{\|d_k\|^2}<\infty.$$

Based on Lemma 3.1, we get the the following results.

Theorem 3.2. Let (H1)-(H2) and the descent condition are satisfied. Considering the conjugate gradient method given by Eqs. (2) and (4), in which α_k is obtained based on Eq. (3). Therefore, we have that either

$$\lim_{k\to\infty}\|g_k\| =0;$$

or

$$\sum_{k=0}^{\infty}\frac{(g_k^T d_k)^2}{\|d_k\|^2}<\infty.$$

Proof. Actually, the conclusion can be proved using the contradiction method. Therefore there is a positivie parameter ε which satisfies

$$\epsilon \leq \|g_k\|. \tag{8}$$

According to Eq. (4), we can get

$$\beta_{k+1} d_k = d_{k+1} + g_{k+1}.$$

So,

$$\beta_{k+1}^2 \|d_k\|^2 - \|g_{k+1}\|^2 - 2 g_{k+1}^T d_{k+1} = \|d_{k+1}\|^2. \tag{9}$$

Therefore,

$$\begin{aligned} \frac{\|d_{k+1}\|^2}{(g_{k+1}^T d_{k+1})^2} &= \frac{\beta_{k+1}^2 \|d_k\|^2}{(g_{k+1}^T d_{k+1})^2} - \left(\frac{1}{\|g_{k+1}\|} + \frac{\|g_{k+1}\|^2}{g_{k+1}^T d_{k+1}}\right)^2 \\ &+ \frac{1}{\|g_{k+1}\|^2} \leq \frac{\beta_{k+1}^2 \|d_k\|^2}{(g_{k+1}^T d_{k+1})^2} + \frac{1}{\|g_{k+1}\|^2} \\ &= \frac{2}{\|g_{k+1}\|^2}. \end{aligned} \tag{10}$$

Then, we obtain

$$\sum_{i=0}^{K} \frac{2}{\|g_i\|^2} \geq \frac{2}{\|g_k\|^2} \geq \frac{\|d_k\|^2}{(g_k^T d_k)^2}. \tag{11}$$

So,

$$\frac{\varepsilon^2}{2K} \leq \frac{(d_k g_k)^2}{\|d_k\|^2}. \tag{12}$$

By using Eqs. (8) and (12), we have

$$\sum_{k=0}^{\infty} \frac{g_k^T d_k}{\|d_k\|^2} = \infty;$$

which immediately contradicts the conclusion of Lemma 3.1. Therefore, Theorem 3.2 is fully proved.

4. APPLICATION

To validate the effectiveness and stability of MCG in reconstructing multi-source loads acting on an airfoil structure, the force reconstruction problem is investigated in the following subsection. Noticing the linear and time-invariant assumptions with regard to load identification, the corresponding convolution equation can be expressed as:[27]

$$y(t) = \int_0^t p(\tau) G(t-\tau) d\tau; \tag{13}$$

in which $y(t)$ denotes the displacement response, $G(t)$ represents the kernel of the impulse response, and $p(t)$ represents the external dynamic force.

The corresponding equally spaced intervals can be obtained using the discretization of the time period, and then we give Eq. (13) in matrix form as:[28–30]

$$G(t)P(t) = Y(t); \tag{14}$$

or given by

$$\begin{pmatrix} y_1 \\ y_2 \\ \vdots \\ y_m \end{pmatrix} = \begin{pmatrix} g_1 & & & \\ g_2 & g_1 & & \\ \vdots & \vdots & \ddots & \\ g_m & g_{m-1} & \cdots & g_1 \end{pmatrix} \begin{pmatrix} p_1 \\ p_2 \\ \vdots \\ p_m \end{pmatrix} \triangle t.$$

Considering the static characteristic of the structure before the force is applied, we can assert that $y_0 = 0, g_0 = 0$, and then G is the lower triangular matrix.

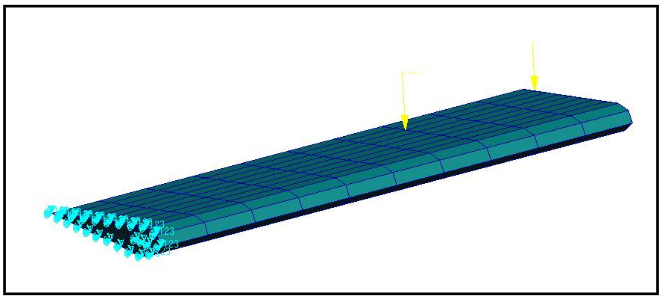

Figure 1. The finite element model of the airfoil.

In order to reconstruct $P(t)$, it is very necessary to get the value of $G(t)$ and $y(t)$. Exploiting the finite element method, we can compute the response at any point and the numerical Green's function. More importantly, it is not easy to get the dynamic force $P(t)$ by a direct inverse operation. In the following part, the proposed method will be used to solve this kind of ill-posed inverse problem about force reconstruction of an airfoil structure and a composite laminated cylindrical shell.

4.1. An Airfoil Structure

A practical engineering problem is investigated to determine vertical forces acting on an airfoil structure as shown in Fig. 1. The density, Poisson's ratio, and elastic modulus of the airfoil structure are $\rho = 8.3 \times 10^3$kg/m^3, $\nu = 0.3$, $E = 3.8 \times 10^{11}$MPa, respectively. On the outer surface of the airfoil structure, there is a vertical concentrated force. The corresponding displacement responses can also be vertically obtained. In addition, one side of the airfoil structure is fixed. The arrows in Fig. 1 denote the corresponding points at which the dynamic loads are acting on the airfoil structure.

The corresponding dynamic forces are expressed as the following formulas:

$$\begin{aligned} F_1(t) &= \begin{cases} q_1 \sin(\frac{2\pi t}{t_d}), & 0 \leq t \leq 2t_d \\ 0, & t < 0 \quad and \quad t > 2t_d \end{cases} \\ F_2(t) &= \begin{cases} 4q_2 t/t_d, & 0 \leq t \leq t_d/4 \\ 2q_2 - 4q_2 t/t_d, & t_d/4 < t \leq 3t_d/4 \\ 4q_2 t/t_d - 4q_2, & 3t_d/4 < t \leq t_d \\ 0, & t > t_d \end{cases} \end{aligned}.$$

in which the parameters $q_i (i = 1, 2), t_d$ are 1000N, 800N, and 0.004s, respectively. The time histories of these two forces are drawn by the software MATLAB in Figs. 2 and 3, respectively. Moreover, the numerical method is used to simulate the response of the test data. Figures 4 and 5 show the displacement responses at nodes 391 and 640, respectively. For the simulation of a practical noisy measurement, the noisy response can be expressed as

$$Y_{err} = rand(-1,1) \cdot std(Y_{cal}) \cdot l_{noise} + Y_{cal},$$

where Y_{cal} and $std(Y_{cal})$ represent the computer generated response and its standard deviation, respectively. l_{noise} and $rand(-1,1)$ represent the noisy level and a random number between $[-1,1]$.

To investigate the reverse computing ability of Landweber, the original conjugate gradient method (FRCG), and MCG, different noise levels such as $5\%, 10\%, 20\%$ and 50% are considered. The other parameters are: $\alpha = 6$ and $\epsilon = 0.33$. The

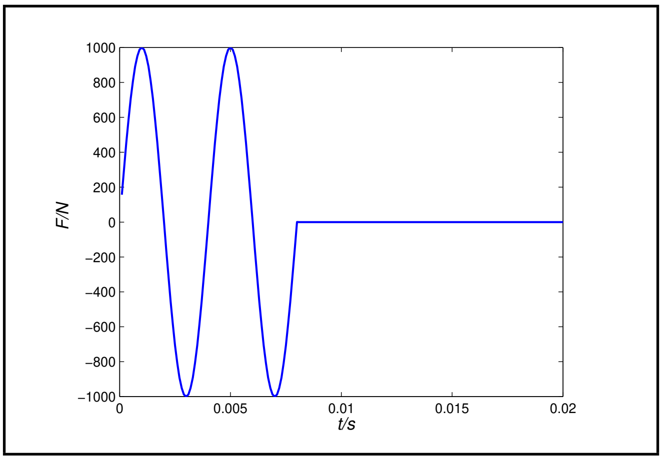

Figure 2. The vertical concentrated sine load acting on the outside surface.

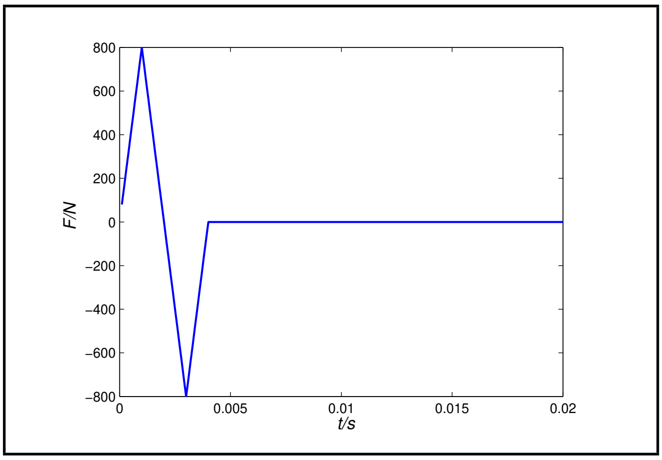

Figure 3. The vertical concentrated triangle load acting on the outside surface.

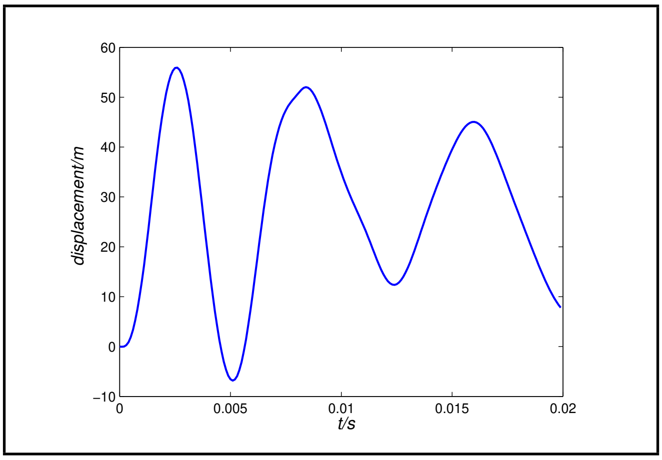

Figure 4. The corresponding vertical displacement response at node 391.

proposed algorithm is used to reconstruct the sine and triangle loads. The performances of the traditional Landweber iteration regularization method, FRCG, and MCG will be compared based on the following relative error

$$\tilde{F} = \|\frac{F_{Real} - F_{Identified}}{F_{Real}}\|. \tag{15}$$

and

$$F_{\text{Average}} = \frac{1}{n}\sum_{i=1}^{n} |\frac{F_{\text{Real}}(i) - F_{\text{Identified}}(i)}{\max\{F_{\text{j}}\}}| * 100; \tag{16}$$

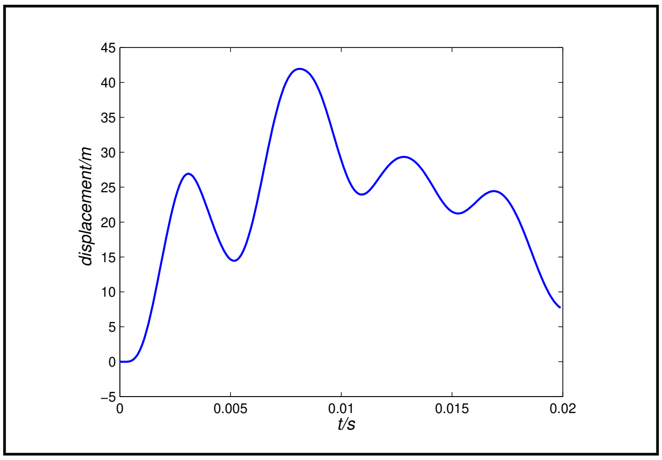

Figure 5. The corresponding vertical displacement response at node 640.

where $i = 1, 2, \cdots, n, j = 1, 2$.

As shown in Fig. 6, under the condition of 5% noise level, Landweber, FRCG, and MCG make good performances in identifying the dynamic force. Landweber's and FRCG's performances are slightly worse than MCG's. Their relative deviations are displayed in Fig. 7. It can be found from these figures that Landweber's and FRCG's errors are much greater than MCG's, which shows the superiority of MCG. Furthermore, as can be seen from Table 1, this conclusion can also be drawn. This is mainly due to the advantage of MCG. As shown in Table 1, most deviations of Landweber and FRCG respectively mainly focus on the range of $11.58\%, 9.80\%$, while most deviations of MCG concentrate in the range of 10.84%. Furthermore, Landweber's maximal deviation and average deviation in identifying the sine force are $7.46\%, 0.91\%$, respectively. FRCG's maximal deviation and average deviation in identifying the sine force are $9.80\%, 2.46\%$, respectively. The average deviation and maximal deviation of MCG in identifying the sine force are $0.88\%, 5.22\%$, respectively. Additionally, this table also shows that Landweber's average and maximal deviation in triangular force recognition are $0.79\%, 11.58\%$, respectively, and FRCG's average and maximal deviation in triangular force recognition are $1.58\%, 8.30\%$, respectively. Those of MCG are $0.76\%, 10.84\%$, respectively. At the same time, the iterative numbers of Landweber and FRCG are 49 and 26, respectively, while the iterative number of the proposed method is 23. In a word, these results above illustrate that the newly developed MCG method achieves good performance and gives stable, effective, and satisfactory results in reconstructing multi-source dynamic loads. Therefore, at other different noise levels, we just compare the performances of the proposed method and the Landweber method in the next part.

As the noise level increases, the identified results slowly get worse, which can be shown in Figs. 8, 9, 10. Their relative deviations are respectively displayed in Figs. 11, 12, 13. It is also noted that the identified results under different noise levels are still good and also acceptable in engineering. These results also show that the proposed algorithm has a powerful identification ability.

As shown in Table 2, under 10% of noise level, most deviations of Landweber mainly focus on the range of 10.22%, while those of MCG concentrate in the range of 9.56%. Additionally, the maximum and mean error of Landweber are

Table 1. The identified force at five time points at noise level 5%.

			Landweber method		MCG method		FRCG method	
	Timepoint	Realforce	Identifiedforce	Error (%)	Identifiedforce	Error (%)	Identified force	Error (%)
Sine	0.001	1000	977.21	2.28	1003.1	0.31	1006.9	0.69
Triangle	0.0006	480	497.29	2.16	492.91	1.61	468.48	1.44
Sine	0.003	-1000	-982.62	1.74	-979.9	2.01	-1037.5	3.75
Triangle	0.001	800	707.37	11.58	713.25	10.84	733.58	8.30
Sine	0.0045	707.11	709.79	0.27	707.68	0.06	756.17	4.91
Triangle	0.0016	320	309.59	1.30	312.52	0.94	300.1	2.49
Sine	0.0063	-453.99	-460.98	0.70	-448.52	0.55	-445.51	0.85
Triangle	0.0033	-560	-568.11	1.01	-569.87	1.23	-565.14	0.64
Sine	0.0073	-891.01	-896.88	0.59	-877.55	1.35	-861.86	2.91
Triangle	0.0038	-160	-135.04	3.12	-134.83	3.15	-157.41	0.32
Error (%)			Maximum	Average	Maximum	Average	Maximum	Average
Sine			7.46	0.91	5.22	0.88	9.80	2.46
Triangle			11.58	0.79	10.84	0.76	8.30	1.58
Iterative steps			49		23		26	

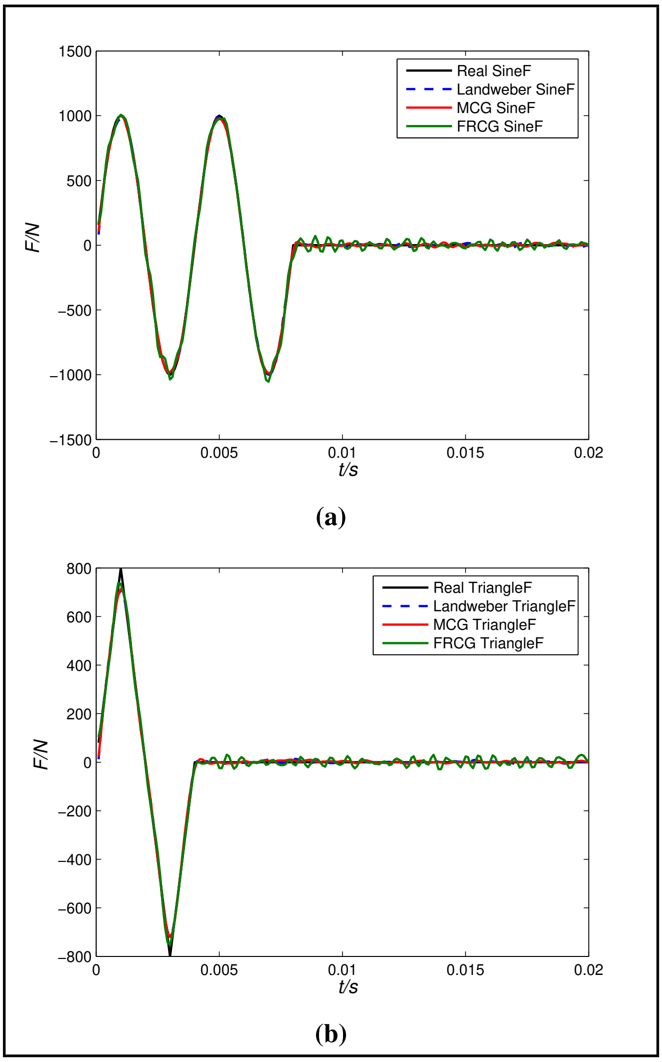

Figure 6. The identified sine and triangle force at noise level 5%; the number of iterations: $N_{Landweber} = 49, N_{MCG} = 23$.

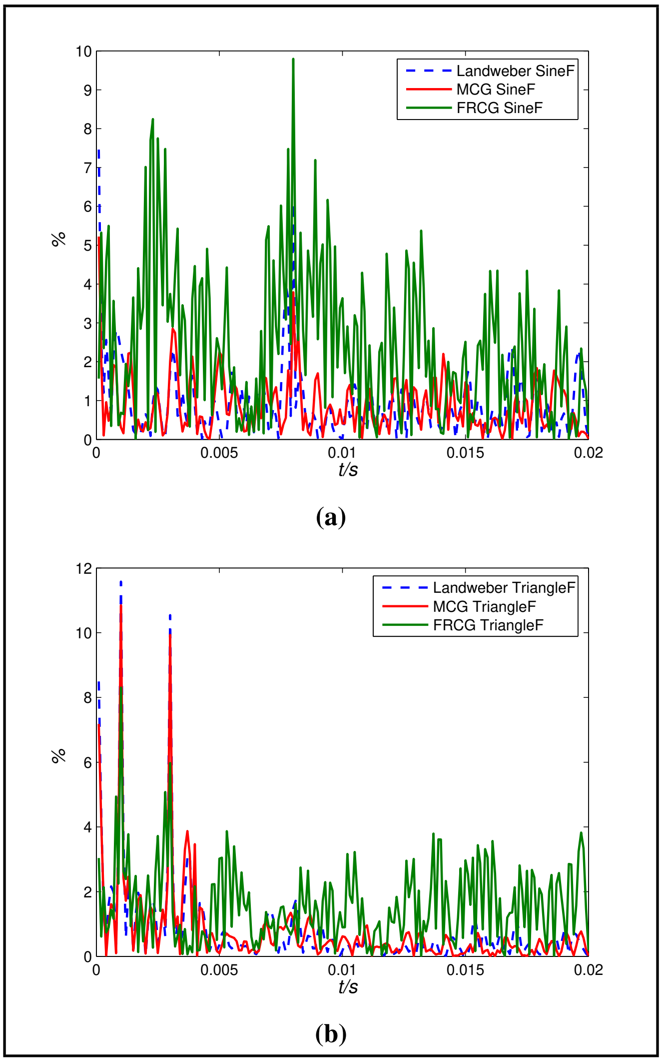

Figure 7. The relative deviations for the identified sine and triangle force at noise level 5%.

6.37%, 1.63%, respectively, and they are much greater than those of MCG in identifying the sine force. Furthermore, the maximal error and average error by MCG are 9.56%, 0.93%, respectively, and they are less than those of Landweber in identifying the triangle force. Besides, the iteration number of Landweber is 62, while that of MCG method is 30.

As shown in Table 3, under 20% of noise level, most deviations of MCG concentrate in the range of 13.16%, which is smaller than Landweber. Additionally, the average and maximal error of Landweber in identifying the sine force are 3.78%, 13.74%, respectively, which are greater than those of MCG (3.32% and 13.16%, respectively). Moreover, in identifying the triangle force, it can also be shown that the average and maximal errors by Landweber are 2.16%, 8.98%, respectively, while those of the present method are 1.76%, 10.21%, respectively. However, the average error is less than that of Landwe-

Table 2. The identified force at five time points at noise level 10%.

			Landweber method		MCG method	
	Timepoint	Realforce	Identifiedforce	Error (%)	Identifiedforce	Error (%)
Sine	0.001	1000	1024.8	2.48	997.68	0.23
Triangle	0.0006	480	492.02	1.50	482.14	0.27
Sine	0.003	-1000	-993.7	0.63	-1041.2	4.12
Triangle	0.001	800	718.26	10.22	723.55	9.56
Sine	0.0045	707.11	689.39	1.77	730.58	2.35
Triangle	0.0016	320	330.82	1.35	305.01	1.87
Sine	0.0063	-453.99	-453.61	0.04	-455.63	0.16
Triangle	0.0033	-560	-587.92	3.49	-583.57	2.95
Sine	0.0073	-891.01	-886.26	0.48	-897.66	0.67
Triangle	0.0038	-160	-151.99	1.00	-147.24	1.60
Error (%)			Maximum	Average	Maximum	Average
Sine			6.37	1.63	5.13	1.46
Triangle			10.22	0.97	9.56	0.93
Iterative steps			62		30	

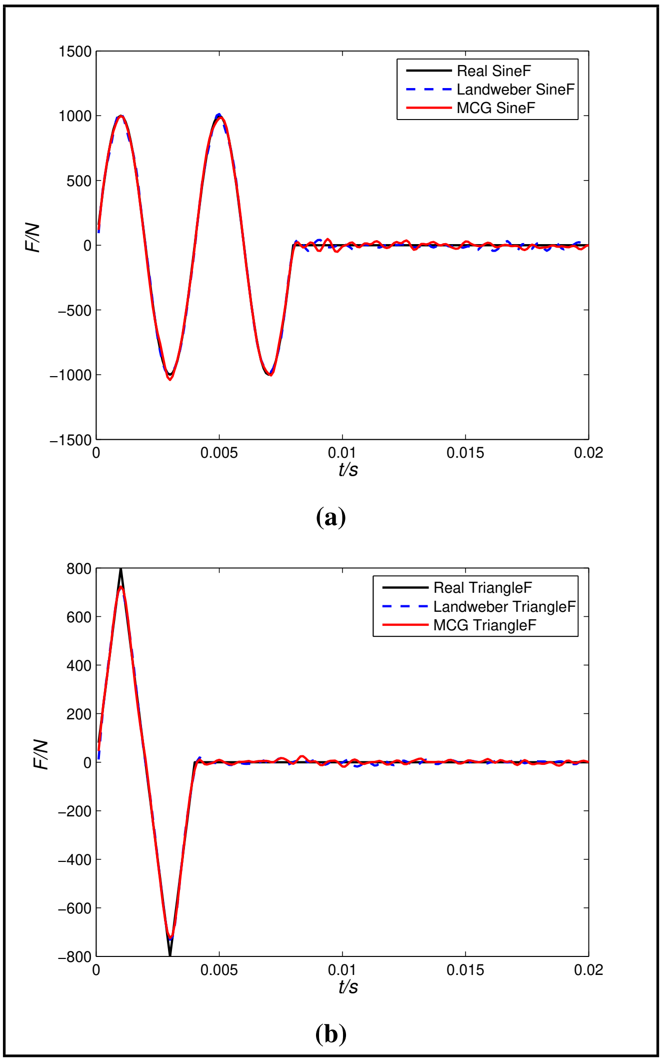

Figure 8. The identified sine and triangle force at noise level 10%; the number of iterations: $N_{Landweber} = 62, N_{MCG} = 30$.

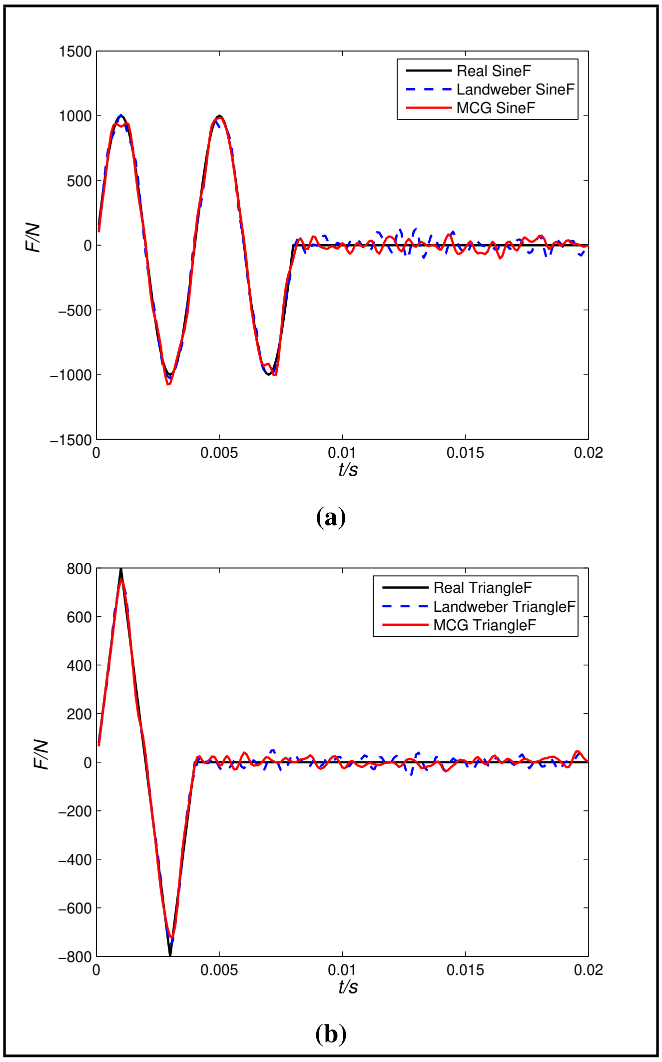

Figure 9. The identified sine and triangle force at noise level 20%; the number of iterations: $N_{Landweber} = 102, N_{MCG} = 33$.

ber's. At the same time, the iteration number of Landweber is 102, while the iteration number of the proposed method is 33.

Table 4 displays the identified performances of Landweber and MCG in detail under 50% of the noise level. It shows that most errors of the present method are less than Landweber, which owes to the stable and efficient identification of the proposed algorithm. As shown in Table 4, most of Landweber's deviations mainly focus on the range of 32.69%, while those of MCG concentrate in the range of 26.90%. Additionally, Landweber's maximum and mean deviations are 32.69%, 9.10%, respectively, much greater than those of MCG in identifying the sine force. Moreover, in the triangle force identification, the average and maximal deviation of MCG are 4.81%, and 15.27%, respectively, but MCG's average deviation is less than Landweber's. Besides, Landweber's iteration number

Table 3. The identified force at five time points at noise level 20%.

			Landweber method		MCG method	
	Timepoint	Realforce	Identifiedforce	Error (%)	Identifiedforce	Error (%)
Sine	0.001	1000	1005.7	0.57	915.48	8.45
Triangle	0.0006	480	476.16	0.48	468.07	1.49
Sine	0.003	-1000	-1028.1	2.81	-1069.2	6.92
Triangle	0.001	800	728.12	8.99	751.99	6.00
Sine	0.0045	707.11	666.44	4.07	664.08	4.30
Triangle	0.0016	320	282.81	4.65	273.89	5.76
Sine	0.0063	-453.99	-463.72	0.97	-488.94	3.50
Triangle	0.0033	-560	-591.35	3.92	-585.15	3.14
Sine	0.0073	-891.01	-932.21	4.12	-1000.9	10.99
Triangle	0.0038	-160	-130.6	3.68	-145.77	1.78
Error (%)			Maximum	Average	Maximum	Average
Sine			13.74	3.78	13.16	3.32
Triangle			8.98	2.16	10.21	1.76
Iterative steps			102		33	

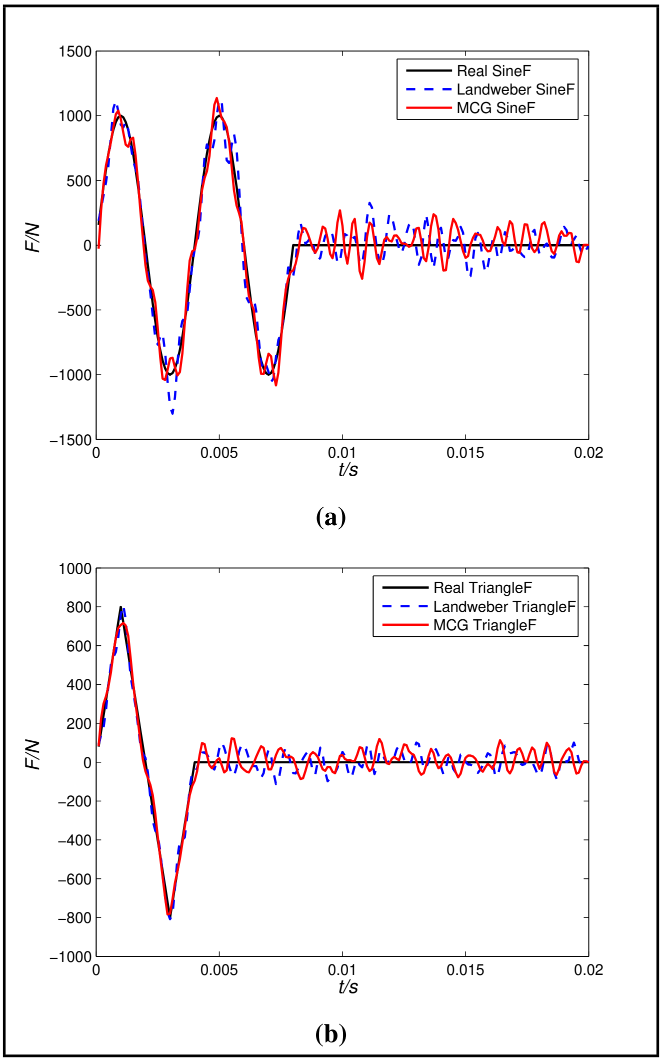

Figure 10. The identified sine and triangle force at noise level 50%; the number of iterations: $N_{Landweber} = 120, N_{MCG} = 38$.

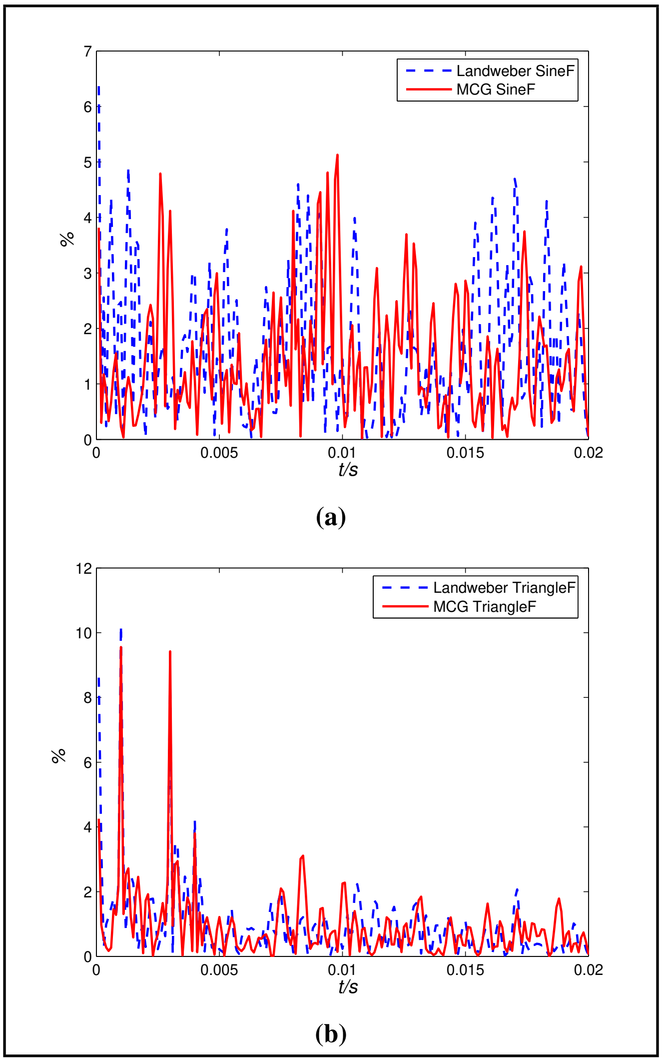

Figure 11. The identified sine and triangle force at noise level 50%; the number of iterations: $N_{Landweber} = 120, N_{MCG} = 38$.

is 120, while that of the MCG method is 38. This further validates that the proposed method is much better.

4.2. A Composite Laminated Cylindrical Shell

Now we will consider a composite laminated cylindrical shell[4] as shown in Fig. 14. We will identify the impact forces acting on this structure by the proposed method. The material properties of the carbon/epoxy and glass/epoxy are shown in Table 5. The radial impact loads act on the outside surface. The measured displacement responses are along the radial direction. One end of the shell structure is free, and the other end is fixed. The arrow in Fig. 14 represents the action point of impact loads. Similarly, as in Section 4.1, the noisy responses with 10% of noise level are computed and displayed in Figs. 15, 16. We reversely compute the impact loads acting

Table 4. The identified force at five time points at noise level 50%.

			Landweber method		MCG method	
	Timepoint	Realforce	Identifiedforce	Error (%)	Identifiedforce	Error (%)
Sine	0.001	1000	930.56	6.94	975.97	2.40
Triangle	0.0006	480	503.65	2.96	463.91	2.01
Sine	0.003	-1000	-1246.4	24.64	-875.46	12.45
Triangle	0.001	800	759.42	5.07	706.05	11.74
Sine	0.0045	707.11	778.07	7.10	571.92	13.52
Triangle	0.0016	320	286.88	4.14	301.42	2.32
Sine	0.0063	-453.99	-413.97	4.00	-449.66	0.43
Triangle	0.0033	-560	-491.92	8.51	-561.1	0.14
Sine	0.0073	-891.01	-863.44	2.76	-1082.8	19.18
Triangle	0.0038	-160	-130.02	3.75	-170.47	1.31
Error (%)			Maximum	Average	Maximum	Average
Sine			32.69	9.10	26.90	8.47
Triangle			14.07	5.07	15.27	4.81
Iterative steps			120		38	

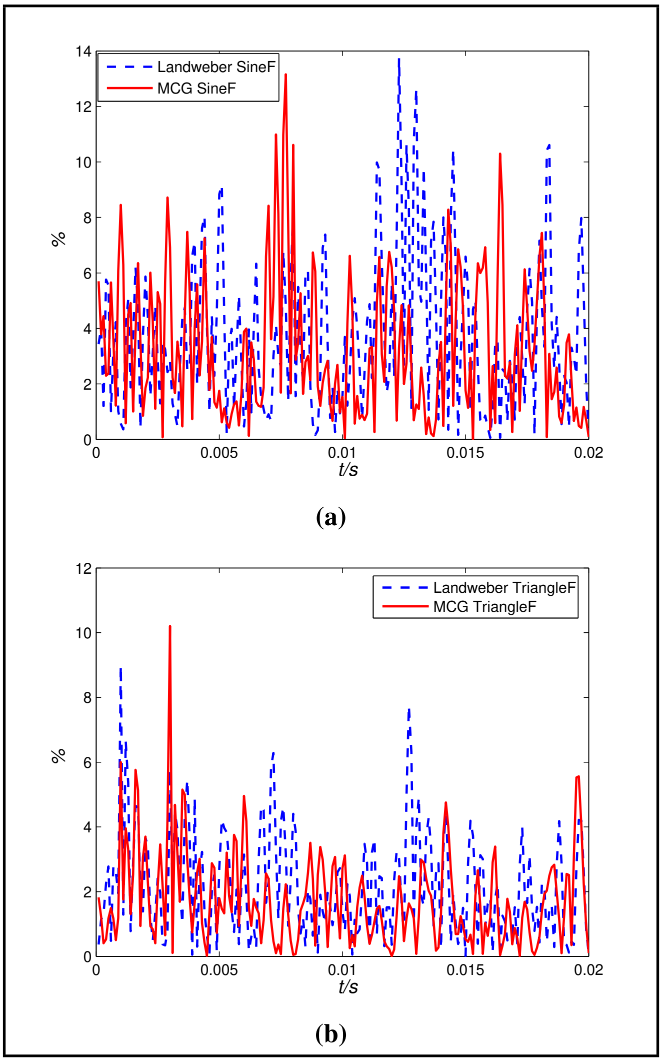

Figure 12. The relative deviations for the identified sine and triangle force at noise level 20%.

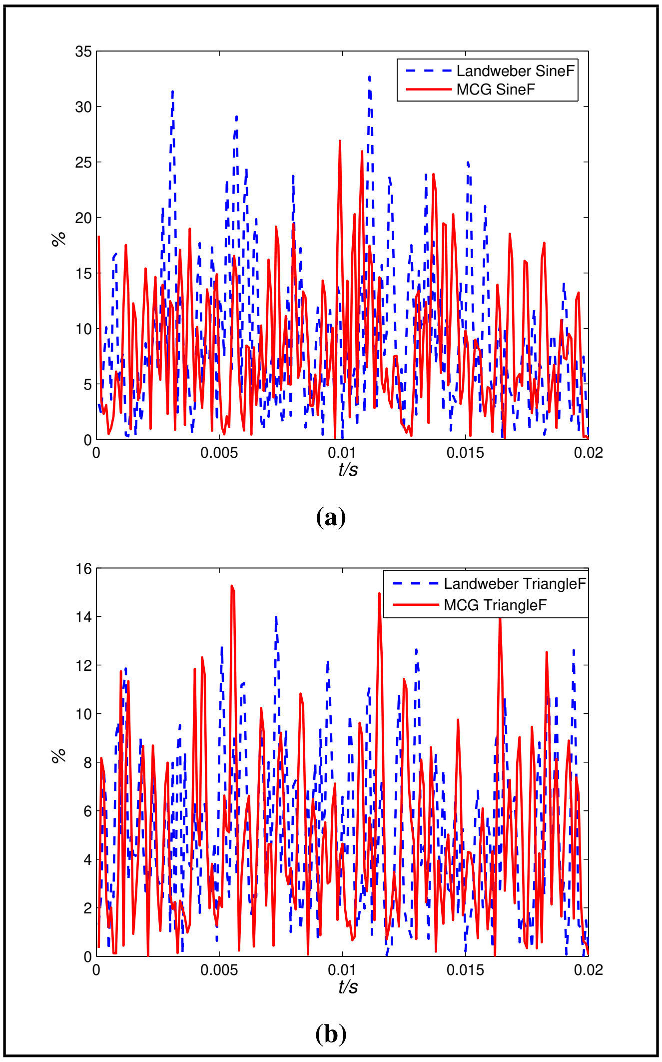

Figure 13. The relative deviations for the identified sine and triangle force at noise level 50%.

on the composite laminated cylindrical shell structure by the Landweber, the original conjugate gradient method (FRCG), and the MCG, and investigate their reverse ability under a noise level of 10%. Additionally, their identified results will also be compared by Eqs. (15) and (16).

As shown in Figs. 17 and 18, under the condition of 10% of noise level, Landweber, FRCG, and MCG perform well in identifying the impact loads. Their relative deviations are displayed in Figs. 19 and 20. It can be seen from these figures that Landweber's and FRCG's error is much greater than MCG's, which shows the superiority of the MCG. As shown in Table 6, most deviations of Landweber and FRCG mainly focus on the range of 22.52%, 25.65%, while most deviations of the MCG concentrate in the range of 20.2%. Furthermore, Landweber's maximal deviation and average deviation in identifying the first impact force are 22.52%, 8.84%, respectively. FRCG's maxi-

Table 5. The material properties of composite laminated cylindrical shell.

Material constants	Material properties of glass/epoxy and carbon/epoxy					
	E_1 (GPa)	E_2 (GPa)	G_12 (GPa)	v_12	v_23	$\rho(\mathrm{gcm}^{-3})$
Glass/epoxv	38.49	9.367	3.414	0.2912	0.5071	2.66
Carbon/epoxy	142.17	9.255	4.795	0.3340	0.4862	1.90

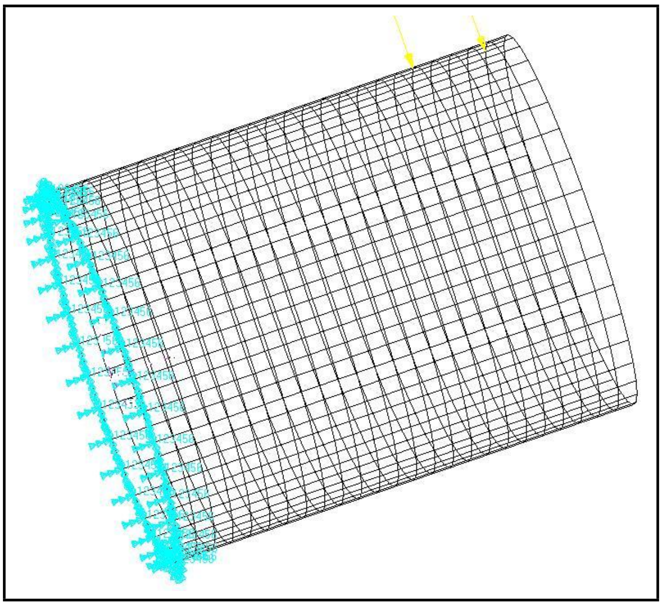

Figure 14. The finite element model of composite laminated cylindrical shell.

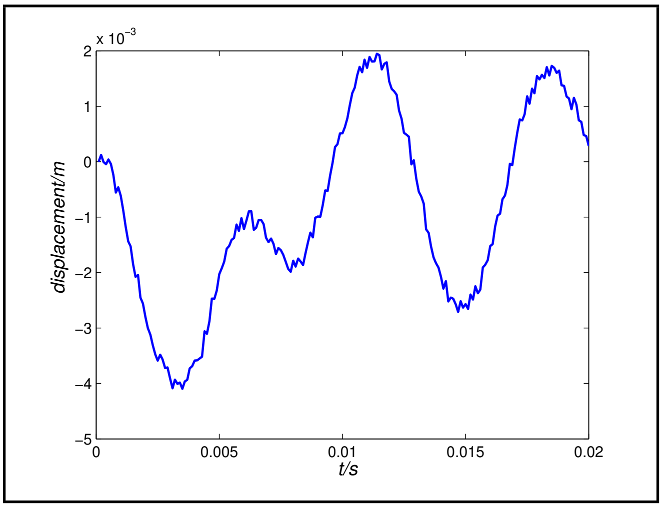

Figure 15. The corresponding radial displacement response.

mal deviation and average deviation in identifying the first impact force are $25.65\%, 8.38\%$, respectively. The average deviation and maximal deviation of MCG in identifying the first impact force are $20.20\%, 7.67\%$, respectively. Additionally, this table also shows that Landweber's and FRCG's average and maximal deviation in the recognition of the second impact force are both larger than MCG's. At the same time, the iterative numbers of Landweber and FRCG are 160 and 108, respectively, while the iterative number of the proposed method is 90. Therefore, these results illustrate that the newly developed MCG method is stable and effective in reconstructing the impact loads.

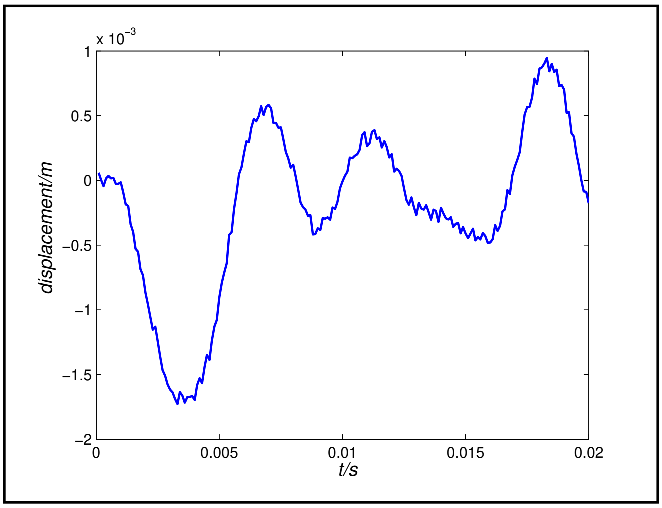

Figure 16. The corresponding radial displacement response.

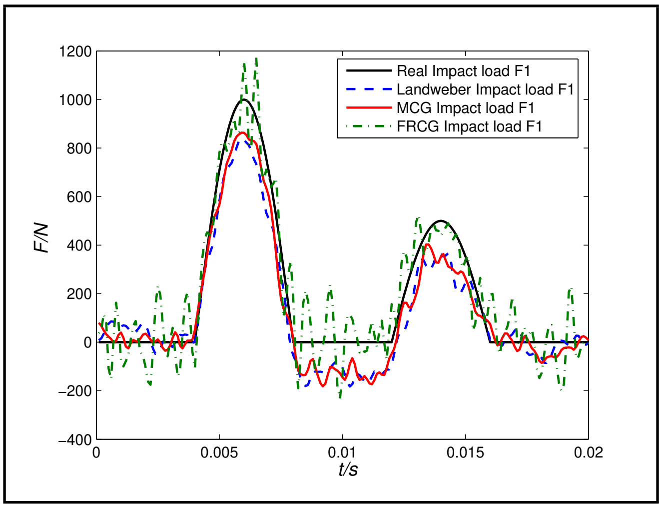

Figure 17. The identified first impact load F_1 at noise level 10%.

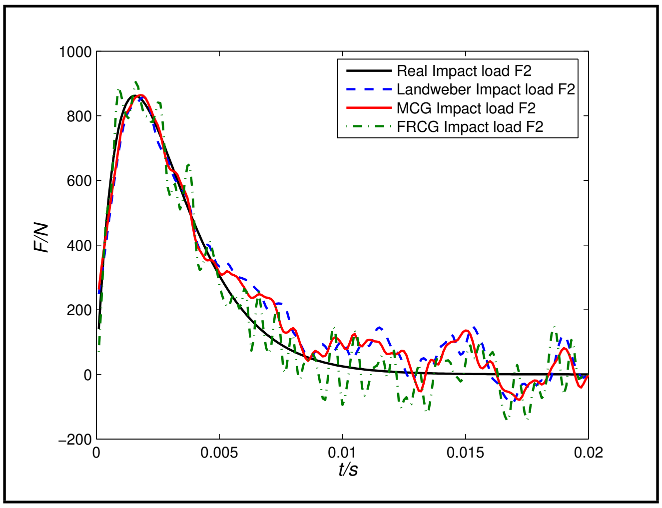

Figure 18. The identified second impact load F_2 at noise level 10%.

Table 6. The identified impact force at five time points at noise level 10%.

			Landweber method		LMCG method		LFRCG method	
	Timepoint	Realforce	Identifiedforce	Error (%)	Identifiedforce	Error (%)	Identified force	Error (%)
Impact load F1	0.0005	0	76.20	7.62	22.71	2.27	-109.25	10.93
Impact load F2	0.0004	464.49	408.79	6.46	435.44	3.37	486.7	2.58
Impact load F1	0.006	1000	833.06	16.69	863.05	13.70	1156.8	15.68
Impact load F2	0.0016	861.97	836.04	3.01	857.81	0.48	904.58	4.94
Impact load F1	0.0122	78.22	3.16	7.51	11.88	6.63	66.24	1.20
Impact load F2	0.0026	738.58	701.87	4.26	746.47	0.92	839.36	11.69
Impact load F1	0.014	500	361.71	13.83	352.51	14.75	438.25	6.18
Impact load F2	0.0102	22.37	75.13	6.12	79.55	6.63	-26.59	5.68
Impact load F1	0.0169	0	31.56	3.16	6.26	0.63	187.36	18.74
Impact load F2	0.0126	5.95	2.33	0.42	59.35	6.20	-70.60	8.88
Error (%)			Maximum	Average	Maximum	Average	Maximum	Average
Impact load F1			22.52	8.84	20.20	7.67	25.65	8.38
Impact load F2			17.09	6.55	15.56	5.82	17.31	6.19
Iterative steps			160		90		108	

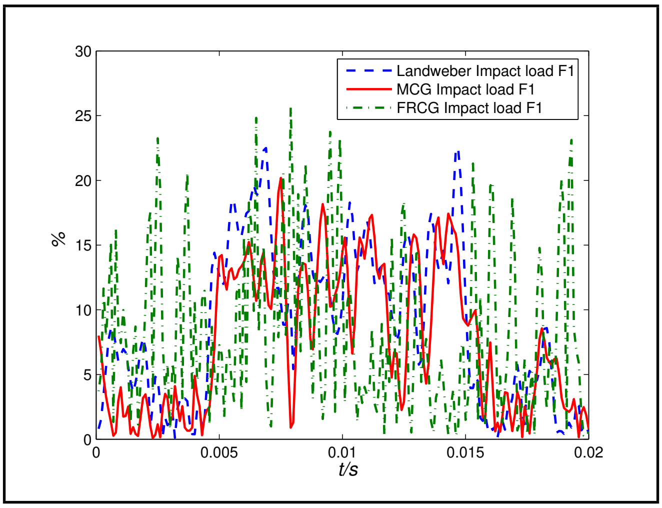

Figure 19. The relative deviations for the identified first impact load F_1 at noise level 10%.

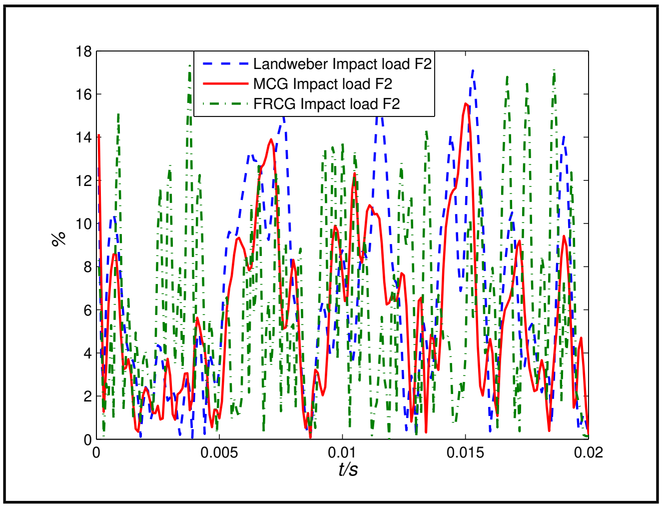

Figure 20. The relative deviations for the identified second impact load F_2 at noise level 10%.

5. CONCLUSION

Dynamic load identification is an important problem in practical structural engineering. The solution to this problem cannot be directly dealt with by the traditional inverse matrix method. In this paper, we have proposed a new fast convergent conjugate gradient algorithm for the dynamic force reconstruction of an airfoil structure and a composite laminated cylindrical shell. Numerical performances have shown that the proposed algorithm is a powerful method for dynamic load identification.

6. ACKNOWLEDGEMENTS

This work was supported by the National Natural Science Foundation of China (51775308), and the Open Fund of Hubei key Laboratory of Hydroelectric Machinery Design and Maintenance (2019KJX12).

REFERENCES

[1] Park, S., Choi, S., Oh, S.T., Stubbs, N. and Song, H.C. Identification of the tensile force in high-tension bars using modal sensitivities, *International Journal of Solids and Structures*, **43**(10), 3185-3196, 2006. https://dx.doi.org/10.1016/j.ijsolstr.2005.06.089

[2] Lourens, E., Reynders, E., Roeck, G.D., Degrande, G. and Lombaert, G. An augmented Kalman filter for force identification in structural dynamics, *Mechanical Systems and Signal Processing*, **27**, 446–460, 2012. https://dx.doi.org/10.1016/j.ymssp.2011.09.025

[3] Lage, Y.E., Maia, N.M.M., Neves, M.M. and Ribeiro, A.M.R. Force identification using the concept of displacement transmissibility, *Journal of Sound and Vibration*, **332**(7), 1674–1686, 2013. https://dx.doi.org/10.1016/j.jsv.2012.10.034

[4] Wang, L.J., Liu, J.W., Xie, Y.X. and Gu, Y.T. A new regularization method for the dynamic load identification of stochastic structures, *Computers and Mathematics with Applications*, **76**, 741–759, 2018. https://dx.doi.org/10.1016/j.camwa.2018.05.013

[5] Wang, L.J., Xie, Y.X., Wu, Z.J., Du, Y.X. and He, K.D. A new fast convergent iteration regularization method, *Engineering with Computers*, **35**, 127–138, 2019. https://doi.org/10.1007/s00366-018-0588-4

[6] Wang, L.J., Han, X., Liu, J. and Chen, J.J. An improved iteration regularization method and application to reconstruction of dynamic loads on a plate, *Journal of Com-

putational and Applied Mathematics, **235**(14), 4083-4094, 2011. https://dx.doi.org/10.1007/s00366-018-0588-4

[7] Naets, F., Cuadrado, J. and Desmet, W. Stable force identification in structural dynamics using Kalman filtering and dummy-measurements, *Mechanical Systems and Signal Processing*, **50–51**, 235–248, 2015. https://dx.doi.org/10.1016/j.ymssp.2014.05.042

[8] Qiao, B.J., Zhang, X.W., Wang, C.X., Zhang, H. and Chen X.F., Sparse regularization for force identification using dictionaries, *Journal of Sound and Vibration*, **368**, 71–86, 2016. https://dx.doi.org/10.1016/j.jsv.2016.01.030

[9] Zhu, T., Xiao, S.N. and Yang, G.W. Force identification in time domain based on dynamic programming, *Applied Mathematics and Computation*, **235**, 226–234, 2014. https://dx.doi.org/10.1016/j.amc.2014.03.008

[10] Liu, J., Meng, X.H., Jiang, C., Han, X. and Zhang, D.Q. Time-domain Galerkin method for dynamic load identification, *International Journal for Numerical Methods in Engineering*, **105**(8), 620–640, 2016. https://dx.doi.org/10.1002/nme.4991

[11] Jacquelin, E., Bennani, A. and Hamelin, P. Force reconstruction: analysis and regularization of a deconvolution problem, *Journal of Sound and Vibration*, **265**(1), 81–107, 2003. https://dx.doi.org/10.1016/S0022-460X(02)01441-4

[12] Law, S.S., Bu, J.Q., Zhu, X.Q. and Chan, S.L. Vehicle axle loads identification using finite element method, *Engineering Structures*, **26**(8), 1143–1153, 2004. https://dx.doi.org/10.1016/j.engstruct.2004.03.017

[13] Gunawan, F.E., Homma, H. and Kanto, Y. Two-step B-splines regularization method for solving an ill-posed problem of impact-force reconstruction, *Journal of Sound and Vibration*, **297**(1–2), 200–214, 2006. https://dx.doi.org/10.1016/j.jsv.2006.03.036

[14] Zhu, X.Q. and Law, S.S. Moving load identification on multi-span continuous bridges with elastic bearings, *Mechanical Systems and Signal Processing*, **20**(7), 1759–1782, 2006. https://dx.doi.org/10.1016/j.ymssp.2005.06.004

[15] Djamaa, M.C., Ouelaa, N., Pezerat, C. and Guyader, J.L. Reconstruction of a distributed force applied on a thin cylindrical shell by an inverse method and spatial filtering, *Journal of Sound and Vibration*, **301**(3–5), 560–575, 2007.

[16] Law, S.S., Bu, J.Q., Zhu, X.Q. and Chan, S.L. Moving load identification on a simply supported orthotropic plate, *International Journal of Mechanical Sciences*, **49**(11), 1262–1275, 2007. https://dx.doi.org/10.1016/j.ijmecsci.2007.03.005

[17] Zhang, J.Y. and Ohsaki, M. Force identification of prestressed pin-jointed structures, *Computers and Structures*, **89**(23–24), 2361–2368, 2011. https://dx.doi.org/10.1016/j.compstruc.2011.07.007

[18] Xie, S.L., Zhang, Y.H., Xie, Q., Chen, C.H. and Zhang, X.N. Identification of high frequency loads using statistical energy analysis method, *Mechanical Systems and Signal Processing*, **35**(1–2), 291–306, 2013. https://dx.doi.org/10.1016/j.ymssp.2012.08.028

[19] Li, Z., Feng, Z. and Chu, F. A load identification method based on wavelet multi-resolution analysis, *Journal of Sound and Vibration*, **333**(2), 381–391, 2014. https://dx.doi.org/10.1016/j.jsv.2013.09.026

[20] Wang, T. Wan, Z. Wang, X. and Hu, Y. A novel state space method for force identification based on the Galerkin weak formulation, *Computers and Structures*, **157**, 132–141, 2015. https://dx.doi.org/10.1016/j.compstruc.2015.05.015

[21] Neubauer, A. On Landweber iteration for nonlinear ill-posed problems in Hilbert scales, *Numerische Mathematik*, **85**(2), 309–328, 2000. https://dx.doi.org/10.1515/jiip-2015-0086

[22] Wang, L.J., Cao, H.P. and Xie, Y.X. An Improved Iterative Tikhonov Regularization Method for Solving the Dynamic Load Identification Problem, International *Journal for Computational Methods in Engineering Science and Mechanics*, **16**(5), 292–300, 2015. https://dx.doi.org/10.1080/15502287.2015.1080318

[23] Jayalakshmi, V. and Rao, A.R.M. Simultaneous identification of damage and input dynamic force on the structure for structural health monitoring, *Structural and Multidisciplinary Optimization*, **55**, 1–28, 2017. https://dx.doi.org/10.1007/s00158-016-1637-5

[24] Maes, K., Nimmen, K.V., Lourens, E., Rezayat, A., Guillaume, P., Roeck, G.D. and Lombaert, G. Verification of joint input-state estimation for force identification by means of in situ measurements on a footbridge, *Mechanical Systems and Signal Processing*, **75**, 245–260, 2016. https://dx.doi.org/10.1016/j.ymssp.2015.12.017

[25] Yuan, G., Lu, S. and Wei, Z. A line search algorithm for unconstrained optimization, *Journal of Software Engineering and Applications*, **3**, 503–509, 2010. https://dx.doi.org/10.4236/jsea.2010.35057

[26] Zoutendijk, G. Nonlinear programming computational methods, in: Abadie J. (Ed.) Integer and nonlinear programming, North Holland, Amsterdam, 1970.

[27] Liu, J., Han, X., Jiang, C., Ning, H.M. and Bai, Y.C. Dynamic Load Identification for Uncertain Structures Based on Interval Analysis and Regularization Method, *International Journal of Computational Methods*, **8**(4), 667–683, 2011. https://dx.doi.org/10.1142/S0219876211002757

[28] Wang, L.J., Xu, L., Xie, Y.X., Du, Y.X. and Han, X. A new hybrid conjugate gradient method for dynamic force reconstruction, *Journal Advances in Mechanical Engineering*, **11**(1), 1–21, 2019. https://dx.doi.org/10.1177/1687814018822360

[29] Wang, L.J., Cao, H.P., Han, X., Liu, J. and Xie, Y.X. An efficient conjugate gradient method and application to dynamic force reconstruction, *Journal of Computational Science*, **8**, 101–108, 2015. https://dx.doi.org/10.1016/j.jocs.2015.03.008

[30] Wang, L.J., Huang, Y., Xie, Y.X. and Du, Y.X. A new regularization method for dynamic load identification, *Science Progress*, **103**(3), 1–15, 2020. https://dx.doi.org/10.1177/0036850420931283